JOURNAL OF VIROLOGY, May 2011, p. 4143–4156 Vol. 85, No. 9
0022-538X/11/$12.00 doi:10.1128/JVI.02606-10

A Rab11- and Microtubule-Dependent Mechanism for Cytoplasmic Transport of Influenza A Virus Viral RNA▽†

Maria Joao Amorim,[1]‡ Emily A. Bruce,[1]‡ Eliot K. C. Read,[1] Ágnes Foeglein,[1] Robert Mahen,[2] Amanda D. Stuart,[1] and Paul Digard[1]*

Division of Virology, Department of Pathology, University of Cambridge, Tennis Court Road, Cambridge CB2 1QP, United Kingdom,[1] and Medical Research Council Cancer Cell Unit, Hutchinson/MRC Research Centre, Hills Road, Cambridge CB2 2XZ, United Kingdom[2]

Received 15 December 2010/Accepted 2 February 2011

The viral RNA (vRNA) genome of influenza A virus is replicated in the nucleus, exported to the cytoplasm as ribonucleoproteins (RNPs), and trafficked to the plasma membrane through uncertain means. Using fluorescent *in situ* hybridization to detect vRNA as well as the live cell imaging of fluorescently labeled RNPs, we show that an early event in vRNA cytoplasmic trafficking involves accumulation near the microtubule organizing center in multiple cell types and viral strains. Here, RNPs colocalized with Rab11, a pericentriolar recycling endosome marker. Cytoplasmic RNP localization was perturbed by inhibitors of vesicular trafficking, microtubules, or the short interfering RNA-mediated depletion of Rab11. Green fluorescent protein (GFP)-tagged RNPs in living cells demonstrated rapid, bidirectional, and saltatory movement, which is characteristic of microtubule-based transport, and also cotrafficked with fluorescent Rab11. Coprecipitation experiments showed an interaction between RNPs and the GTP-bound form of Rab11, potentially mediated via the PB2 subunit of the polymerase. We propose that influenza virus RNPs are routed from the nucleus to the pericentriolar recycling endosome (RE), where they access a Rab11-dependent vesicular transport pathway to the cell periphery.

Influenza A virus is a ubiquitous pathogen of homeothermic vertebrates with the capacity to cause seasonal epidemics and occasional, potentially devastating outbreaks in humans (55). The virus has a single-stranded RNA genome split into eight segments that encode between 10 and 12 polypeptides depending on the virus strain (61). The viral RNA (vRNA) segments are encapsidated into ribonucleoprotein (RNP) particles by the viral RNA-dependent RNA polymerase and a single-strand RNA-binding protein, NP (40). Once delivered to the cell nucleus at the start of infection, they act as independent units for the purposes of transcription and replication of the virus genome. Virus assembly subsequently takes place at the apical plasma membrane of infected cells; here, the three viral membrane proteins (HA, NA, and M2) join with the M1 matrix protein, small amounts of the NEP/NS2 protein, and the RNPs to form new enveloped virus particles through a process of budding. This assembly phase of the virus life cycle is not especially well understood but is thought to result from a cascade of protein-protein interactions between the viral components, as well as probable RNA-RNA interactions between specific vRNAs that ensure a complete genome is incorporated (27, 36). Unlike many other enveloped viruses, the formation of a mature virus particle does not depend on the cellular ESCRT pathway (11, 15, 58) but requires the function of the small GTPase Rab11 (10) and the viral M2 protein (48).

A further aspect of the viral life cycle that is imperfectly understood concerns the intracellular trafficking of the viral genome. The nuclear export of newly synthesized RNPs involves sequential interactions between the RNPs, M1, and NEP and the cellular nuclear export factor Crm1 (8). However, the mechanisms that then transport RNPs across the cytoplasm to the sites of budding at the apical plasma membrane are poorly defined. Individual RNPs range in size from ~2.5 to 6 MDa (depending on the length of the vRNA segment), and thus simple diffusion is unlikely to operate over long distances. On general principles, as well as precedents from other viruses (41), the involvement of one or more arms of the cytoskeleton seems likely. Although NP has been defined as an actin-binding protein (19) and shown to partially colocalize with actin at the plasma membrane (5, 53), direct evidence for a role in RNP transport is lacking. Instead, an intact cortical actin web seems to be required to support filamentous viral budding (47, 53). Cytoplasmic RNPs have been suggested to colocalize with microtubules (34), but although (like actin) tubulin has been found to copurify with RNPs and be present in virions (31, 52), direct evidence for a role in trafficking is sparse. In general, pharmacologic interference with the cytoskeleton (after virus entry) has relatively slight effects on influenza A virus replication outside certain drugs that also interfere with viral protein synthesis (4, 22, 34, 45, 47, 50, 53). Thus, this aspect of the virus life cycle has many unresolved questions.

Here, we provide positive evidence that the transport of the viral genome from the nucleus to the cell periphery does indeed involve the microtubule network. Furthermore, we provide a new model for efficient RNP transport that involves the

* Corresponding author. Mailing address: Division of Virology, Department of Pathology, University of Cambridge, Tennis Court Road, Cambridge CB2 1QP, United Kingdom. Phone: 44 1223 336920. Fax: 44 1223 336926. E-mail: pd1@mole.bio.cam.ac.uk.

† Supplemental material for this article may be found at http://jvi.asm.org/.

‡ These authors contributed equally to the manuscript.

▽ Published ahead of print on 9 February 2011.

piggybacking of RNPs onto the vesicular transport network at the pericentriolar RE via an interaction between PB2 and Rab11.

MATERIALS AND METHODS

Cells, viruses, and drugs. Human embryonic kidney 293T, Madin-Darby canine kidney (MDCK), and human alveolar basal epithelial cells (A549) were cultured as previously described (12). Two subtypes of human virus were used, A/Puerto Rico/8/34 (PR8; H1N1) and A/Udorn/301/72 (Udorn; H3N2) (47), as well as A/duck/Eng/8/1/1962 (Duck/Eng; H4N6) (24) and A/Eq/Newmarket/11/03 (Eq/Nkt; H3N8) (gift of Janet Daly). Virus infections were carried out at a multiplicity of infection (MOI) of 5 to 10 in serum-free medium. Drugs were from Sigma and were used at 20 (nocodazole), 150 (monensin), 5 (demecolcine), or 10 μM (paclitaxel) final concentrations.

Plasmids and transfections. A plasmid encoding green fluorescent protein (GFP)-tagged constitutively active (CA) (Q67L) Rab8 protein was a gift of Folma Buss (49). GFP-tagged wild-type (WT) and CA (Q70L) Rab11a and CA (Q67L) Rab4 constructs are described elsewhere (10, 16, 51). mCherry-C2 versions of both Rab11 proteins were created by PCR amplifying and cloning the Rab11a genes into EcoRI and BamHI sites in the polylinker of an mCherry version of pEGFP-C2 from Clontech. Primers TCGAGAATTCATGGGCACCCGCG (rab11aF) and TCGAGGATCCTTAGATGTTCTGACAGCACTGCA (rab11aR) were used. pCDNA3 plasmids used to synthesize fluorescent *in situ* hybridization (FISH) probes to detect vRNA from segments 1, 2, 4, and 7 are described elsewhere (2, 23, 35). Plasmids used for the minireplicon system are described in reference 35, except for GFP-NP (29) and pPolI segments 7 and 8 (17). To reconstitute GFP-tagged RNPs, 1×10^5 293T cells were transfected with pcDNA3 PB1, PB2, PA (130 ng each), NP (80 ng), GFP-NP (50 ng), and pPolI segments 7 and 8 (130 ng each) using Lipofectamine 2000 (Invitrogen) according to the manufacturer's instructions, incubated overnight, and imaged around 24 h later. The treatment of cells with short interfering RNAs (siRNAs) against Rab11a and Rab11b or with nontargeting siRNAs was carried out as previously described (10).

Microscopy. FISH analysis was performed essentially as described in reference 2. To generate FISH probes, pCDNA3 plasmids containing segments 1, 2, 4, or 7 were cut with XbaI and transcribed as described previously (42), except that T7 RNA polymerase was used to produce a positive-sense probe to detect vRNA. Probes were directly labeled using cyanine 5-UTP (Perkin Elmer) or ChromaTide Alexa Fluor 488-5-UTP (Invitrogen). Immunofluorescence was carried out as described previously (53). Reagents included mouse monoclonal antibody to γ-tubulin (ab11316; Abcam), sheep polyclonal antibody to TGN46 (AHP500G; AbD-Serotec), rabbit polyclonal anti-NP (2915) (37), rat monoclonal antibody to α-tubulin (YL1/2 MCA77G; AbD-Serotec), and mouse monoclonal antibody to GM130 (610822; BD Transduction Laboratory).

For live imaging, cells were grown in chambered glass-bottomed dishes (Lab-Tek) and maintained at 37°C in Leibovitz L-15 CO_2-independent medium (Gibco) during imaging. Samples were imaged using Zeiss LSM510 or Leica SPE or TCS-NT confocal microscopes and postprocessed using Adobe Photoshop and ImageJ (NIH). Unless otherwise stated, single optical sections are shown. Particle-tracking analysis was done using the MtrackJ plugin (32). Colocalization analysis was done using the intensity correlation analysis WCIF plugin (http://www.uhnresearch.ca/facilities/wcif/imagej/appendix_1.htm).

For fluorescence recovery after photobleaching (FRAP) analysis, cells were imaged on a Zeiss LSM 510 confocal microscope using a 63× magnification, 1.4-numeric-aperture objective. Photobleaching was performed using 100% power from a 30-mW 488-nm laser line running at 6.1 A within a 1.7- by 1.7-μm square, which took a total of 0.5 s. Images were captured at 0.7% of laser output at 0.25-s intervals, obtaining 512- by 512-pixel images. Samples were corrected for background fluorescence and acquisition photobleaching as described previously (29). The averages of multiple individual cells are presented.

The Duolink II fluorescent proximity assay (Olink Bioscience) was used in conjunction with standard confocal microscopy to detect epitopes within an ~40-nm distance (54). Samples were fixed, permeabilized, and stained with primary antibodies as described above and then stained with oligonucleotide-labeled secondary antibodies. Samples were treated with a ligation solution (allowing nearby oligonucleotide probe pairs to form a closed circle), and an amplification solution containing polymerase and fluorescently labeled oligonucleotides was added, allowing rolling-circle amplification and the detection of a discrete fluorescent spot (according to the Duolink II fluorescence user manual). Signal was expressed as the number of fluorescent dots per cell in a given field of view and compared to the background signal observed in mock-infected cells and cells treated with one relevant and one irrelevant antibody.

Pulldowns and Western blotting. Pulldowns of GFP-tagged proteins were performed using GFP-Trap beads (Chromotek). Confluent 6-well dishes of 293T cells were transfected with 350 ng of each plasmid and, where applicable, were infected 48 h later with virus for 6 h. Cells were lysed in 500 μl of 50 mM Tris-HCl, pH 8, 25% glycerol, 0.5% NP-40 substitute (Fluka), 200 mM NaCl, 1 mM dithiothreitol (DTT), 1 mM phenylmethylsulfonyl fluoride (PMSF), and protease inhibitor cocktail (Roche) on ice for 30 min. Clarified samples then were preabsorbed on glutathione Sepharose beads (Amersham Biosciences) for 30 min, and the supernatant was bound to GFP-Trap beads for 2 h at 4°C. Beads were washed before and after sample binding with 10 mM Tris HCl, pH 8, 0.1% NP-40 substitute, 150 mM NaCl, 0.5 mM EDTA, 1 mM PMSF, and protease inhibitor cocktail. Bound proteins were eluted by being boiled in SDS-PAGE sample buffer. Bound RNA was extracted by adding 1 ml of Trizol (Invitrogen) and 200 μl chloroform directly to the Trap beads and recovered by ethanol precipitation. Specific RNA species were detected by reverse transcriptase-radiolabeled primer extension followed by urea-PAGE and autoradiography essentially as described previously (35, 46). Western blotting was performed according to standard procedures and imaged using a LiCor Biosciences Odyssey near-infrared platform as described previously (11). Antibodies used included mouse monoclonal antibodies against Rab11a (ab78337; AbCam), GFP (JL8; 632380; Clontech), and influenza M2 (14C2; ab5416; AbCam), rat monoclonal alpha tubulin (YL1/2 MCA77G; AbD-Serotec), and rabbit polyclonal antisera to whole PR8 virions PR8 M1 (A2917) (2), PB1 (V19), PA (V35) (18), PB2 (2N580) (39), and NP (2915) (37).

RESULTS

The influenza virus genome is not thought to exist normally as naked RNA but rather as encapsidated RNP particles containing one copy of a trimeric RNA polymerase and multiple copies of the nucleoprotein (40). Accordingly, the majority of studies that have investigated the localization of the viral genome in cells by microscopy have utilized indirect immunofluorescence against NP as a proxy marker for vRNA. However, our recent development of FISH protocols for the direct detection of influenza virus RNAs (2, 26, 42) allow more direct visualization of genome trafficking.

We carried out a time course experiment in which MDCK cells were fixed and stained at various times postinfection (p.i.) for vRNA from segments 1 and 4. Early in infection, obvious vRNA staining of the nucleoplasm but not the nucleoli was apparent (Fig. 1A, 5 h). At later times, staining became increasingly biased toward the cytoplasm, such that by 12 h p.i. many nuclei appeared empty of vRNA (Fig. 1A). This time-dependent shift from predominantly nuclear to predominantly cytoplasmic localization is broadly consistent with that expected from the immunofluorescent staining of NP (9, 21, 30). However, at intermediate times postinfection, many cells also showed bright perinuclear foci of vRNA (Fig. 1A, arrows). Similar perinuclear accumulations of vRNA were seen in other cell types, including A549 cells (see later) and 293T cells (Fig. 1B). The perinuclear accumulation of NP has been noted previously (10, 34), and consistently with this information, the structures seen here contained both vRNA and NP, although the FISH staining of the viral genome generally was proportionally more intense (Fig. 1B). The examination of Z-stack animations of serial planes of focus taken throughout the body of the cells showed that these perinuclear foci contained more than one segment and tended to be around the midline of the cell or slightly higher, but they were below the level of the plasma membrane (see Movie S1 in the supplemental material). When

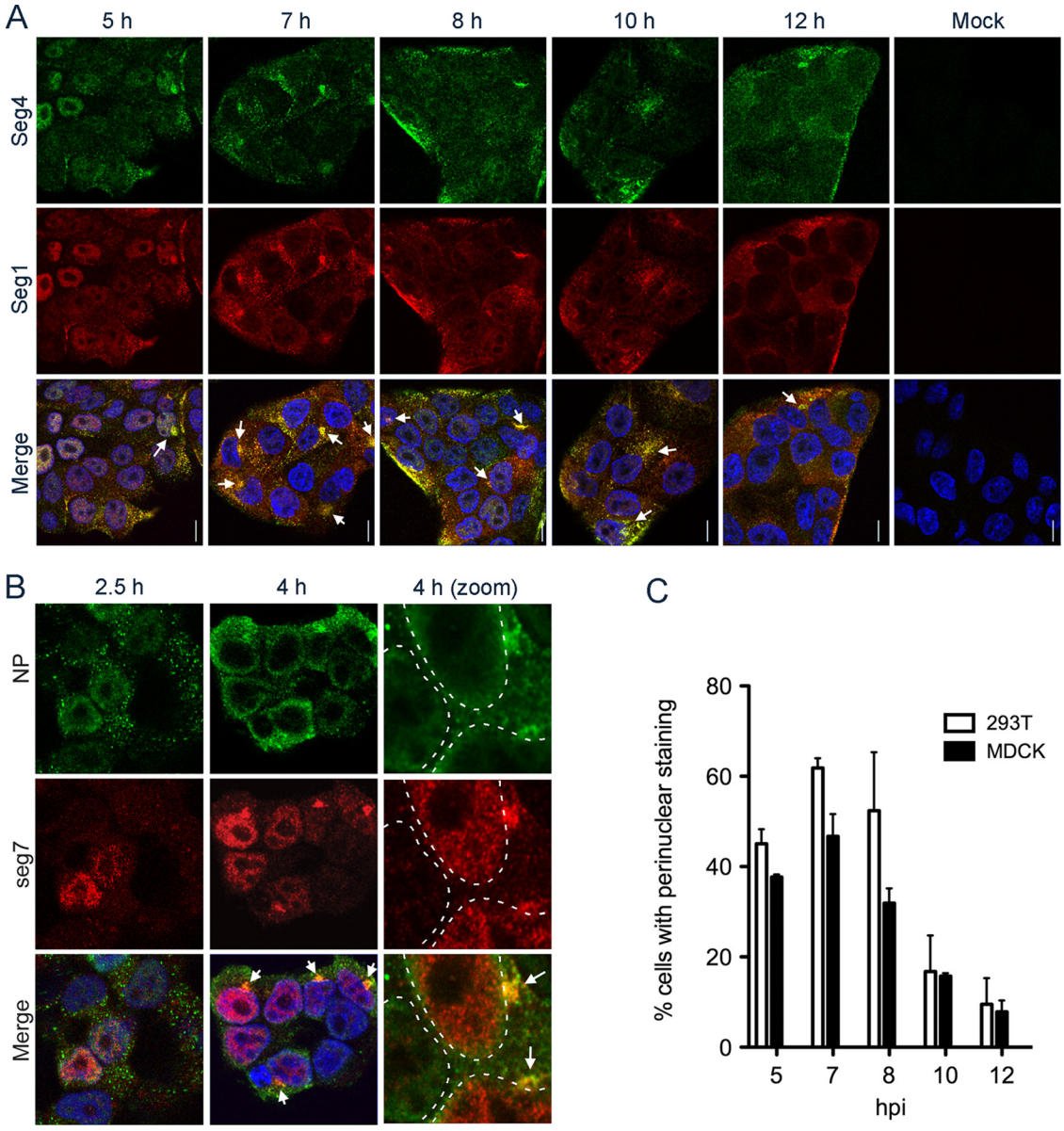

FIG. 1. Time course of vRNA localization in infected cells shows the perinuclear accumulation of vRNA at intermediate times postinfection. MDCK (A) or 293T (B) cells were infected (or mock infected) with PR8 virus and fixed and stained for specific vRNA segments (A) and both vRNA segments and NP (B) at the indicated times p.i. Merged images also include 4′,6′-diamidino-2-phenylindole (DAPI) staining (blue) except in the higher-magnification images in panel B, where for clarity the outline of the DAPI staining is indicated by dashed white lines. (C) The percentage (means ± SE) of cells showing an obvious perinuclear accumulation of vRNA was scored at various times p.i. A minimum of 200 cells from three independent experiments were counted. Also see Movie S1 in the supplemental material.

multiple cells were examined from replicate experiments and scored according to whether perinuclear vRNA staining was present, it was apparent that these structures appeared soon after the onset of vRNA nuclear export and reached a maximum around 7 h p.i., and although they sometimes persisted throughout infection, they generally became less prominent later in infection (Fig. 1C).

To investigate this perinuclear accumulation further, we first asked whether it was a feature of influenza viruses in general or specific to the PR8 strain. We also tested whether the perinuclear body represented a specific cellular location by staining the microtubule organizing center (MTOC) with anti-γ-tubulin. As before, 293T cells infected with PR8 virus contained a prominent perinuclear focus of vRNA staining at 6 h p.i. that, under high magnification, was seen to consist of punctate dots surrounding the MTOC (Fig. 2). This was a common occurrence, as 45 of 51 infected cells examined from two independent experiments displayed this pattern of localization. Similar structures that in all cases surrounded the γ-tubulin staining also were seen in cells infected with the human H3N2 Udorn strain as well as with a low-pathogenicity Duck/Eng H4N6 avian virus and the H3N8 equine influenza virus strain Eq/Nkt

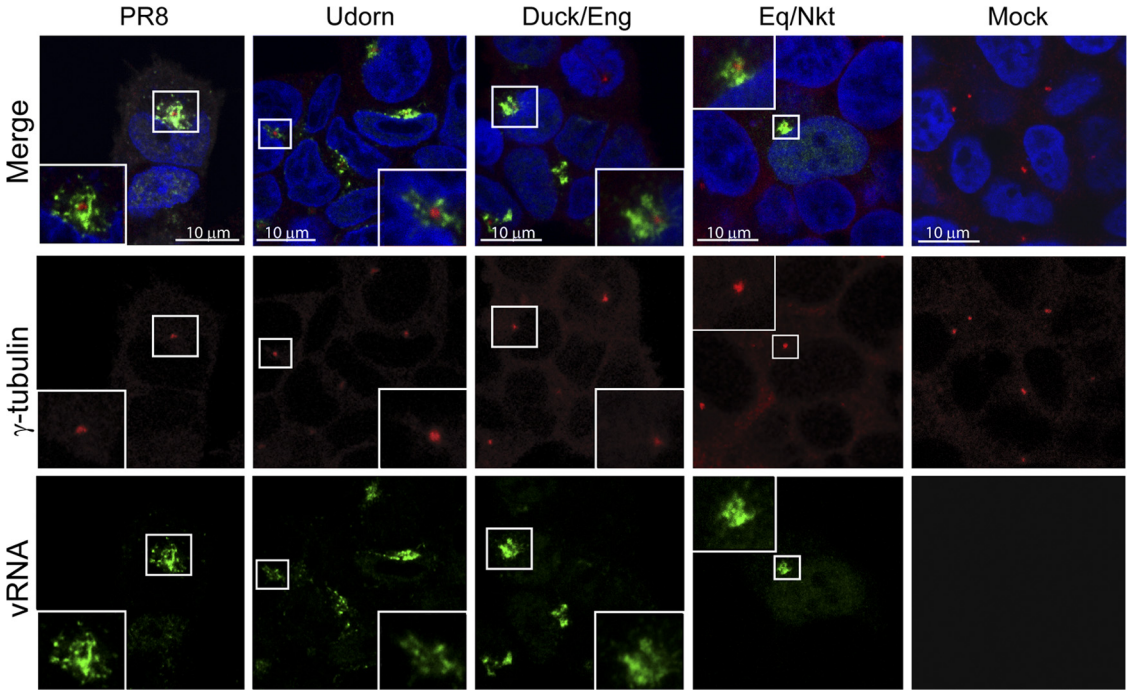

FIG. 2. Perinuclear accumulation of vRNA is a general feature of influenza A viruses. 293T cells were infected (or mock infected) with the indicated viruses, fixed at 6 h p.i., and stained for segment 7 vRNA and γ-tubulin. Merged images include a 4′,6′-diamidino-2-phenylindole (DAPI) channel shown in blue. Insets show higher-magnification images of the boxed areas.

(Fig. 2). The same outcome was obtained when the experiment was repeated with MDCK cells (data not shown).

The consistent localization of vRNA around the MTOC suggested its interaction with one or more of the similarly localized cellular organelles; this was investigated by double staining for components of cellular vesicular transport pathways. Little colocalization (Pearson correlation coefficient of 0.068 ± 0.008, from four fields of view) was seen between perinuclear vRNA and GM130, a marker for the *cis*-Golgi network (Fig. 3A). A similar result (Pearson coefficient of 0.179 ± 0.06, $n = 3$) was obtained when TGN46 was used as a marker for the *trans*-Golgi compartment, and although both vRNA and the cellular protein distributed as a pattern of perinuclear spots, the examination of high-magnification images showed that these patterns were distinct and largely separate (Fig. 3A, inset). A similar lack of colocalization was obtained when EEA1, a marker for early endosomes, or calnexin, a marker for the endoplasmic reticulum, were compared to vRNA (Pearson coefficients of 0.037 ± 0.03, $n = 3$, and 0.087 ± 0.05, $n = 3$, respectively; image data not shown). We have shown previously that cytoplasmic NP colocalizes with Rab11, including at a perinuclear structure (10). Unfortunately, the epitopes seen by our Rab11 antisera did not survive the FISH process (data not shown), making it impossible to test whether vRNA also colocalized with the endogenous protein. However, when a transfected GFP-tagged constitutively active Rab11 (GFP-Rab11 CA) (16) was used as a marker for the RE, a high degree of colocalization was seen with the perinuclear foci of vRNA (Fig. 3B). The Pearson coefficient for vRNA (CA Rab11; 0.541 ± 0.05, $n = 4$) was significantly higher ($P < 0.0001$) than the overlap seen for TGN46 or the other cellular markers. This degree of colocalization also was maintained when more dispersed cytoplasmic foci of vRNA were examined at a later time point (Fig. 3B, 12 h).

The colocalization of vRNA with Rab11-positive structures near the MTOC soon after the onset of genome replication and nuclear export suggested that cytoplasmic vRNA trafficking involves the cellular vesicular transport pathway and therefore the microtubule network. Accordingly, we tested the effects of the pharmacological disruption of these processes on vRNA localization. In untreated MDCK cells, the viral genome was predominantly cytoplasmic late in infection, concentrating at the apical plasma membrane, while NP showed a similar distribution but with additional bright foci in the nuclei (Fig. 4A). Treatment with the microtubule-depolymerizing agent nocodazole led to the loss of the apical polarization of vRNA and NP, and instead optical sections through the midline of the cells showed their pronounced accumulation at lateral membranes. A similar outcome of aberrant vRNA localization to lateral membranes was seen with demecolcine, another drug that destablizes microtubules, as well as when cells were treated with paclitaxel, a microtubule-stabilizing agent, but instead of localizing to lateral membranes it formed prominent aggregates toward the cell periphery. The disruption of vesicular trafficking with the ionophore monensin also altered vRNA trafficking, leading to a persistence of the prominent perinuclear foci of vRNA staining normally seen earlier in infection, as well as a degree of NP nuclear retention. We also examined the effect of the drugs on virus replication by titrating released virus from the cell supernatants. This showed modest but consistent decreases of around 4-fold after drug treatment (Fig. 4B). The Western blot analysis of selected virus

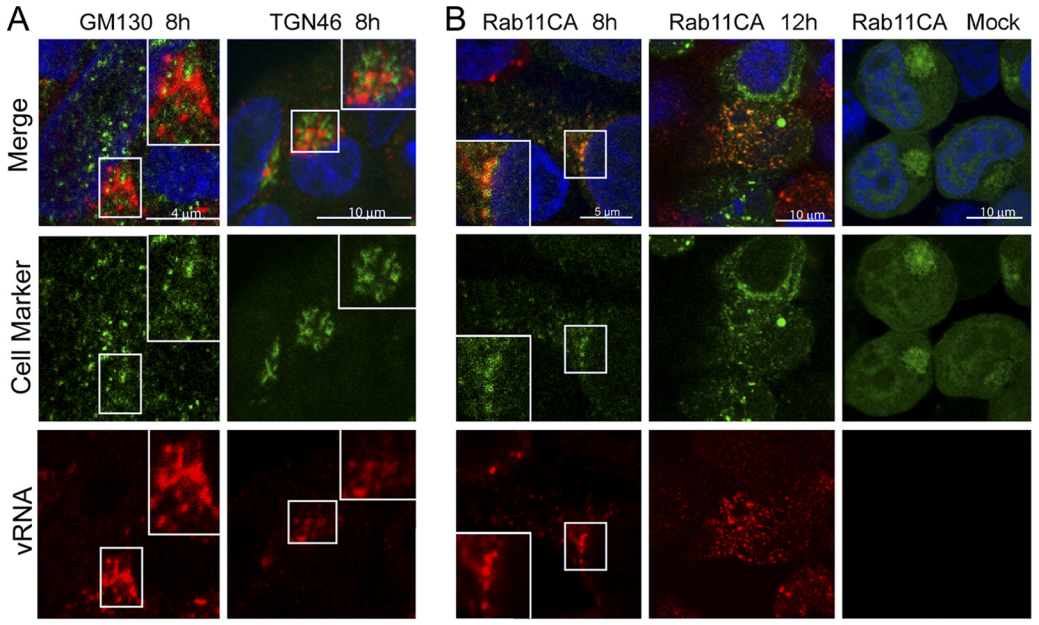

FIG. 3. Relationship of the perinuclear accumulation of vRNA to cellular structures. (A and B) 293T cells were infected with PR8 virus, fixed at the times shown, and stained for segment 7 vRNA (A) and the indicated cellular polypeptides. (B) The cells first were transfected with GFP-Rab11 CA, which was detected by GFP fluorescence. Merged images include a 4′,6′-diamidino-2-phenylindole (DAPI) channel shown in blue. Insets show higher-magnification images of the boxed areas.

polypeptides showed no major effect on viral protein accumulation (Fig. 4C). Overall, these data are consistent with cytoplasmic vRNA trafficking involving the microtubules and the cellular vesicular transport pathway.

To further investigate the hypothesis that RNP cytoplasmic trafficking involves the microtubule network, we established a system in which the movement of RNPs could be investigated in living cells using GFP-tagged NP. Because of the difficulty of

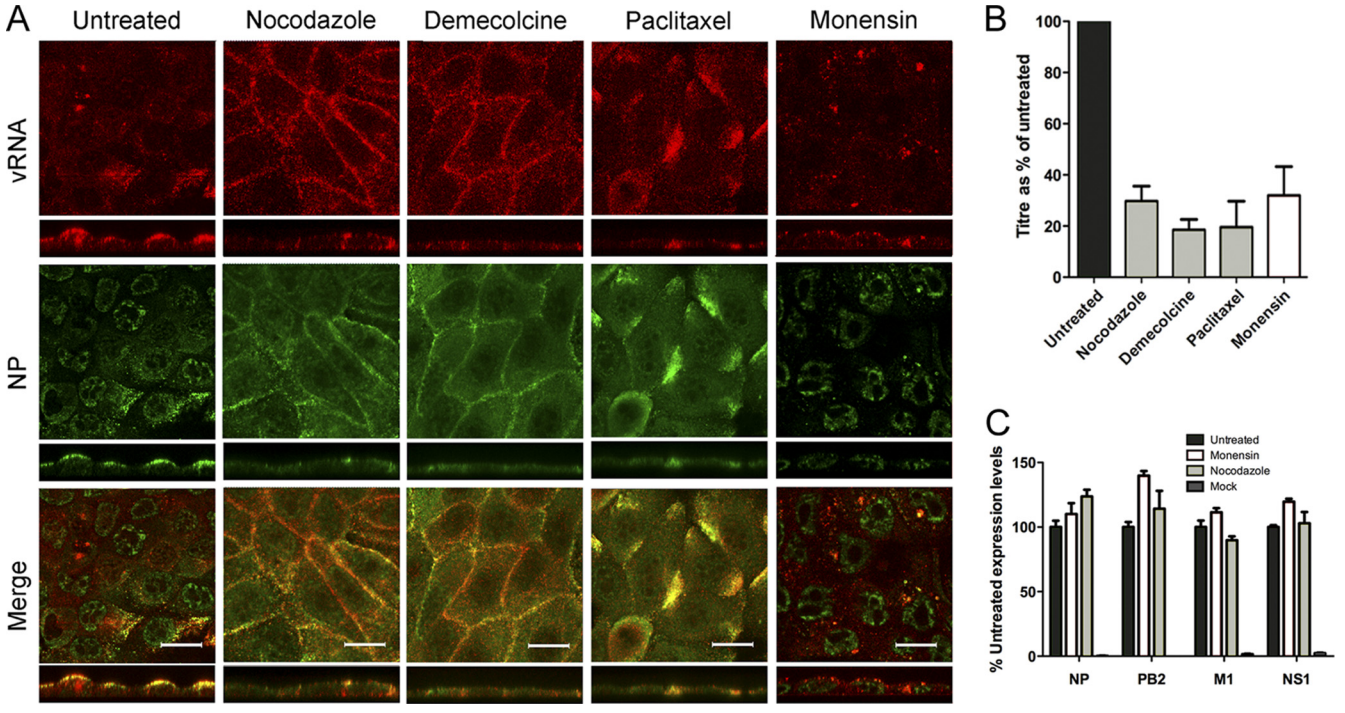

FIG. 4. Effect of inhibitors of cellular trafficking on RNP localization. MDCK cells were infected with PR8 virus and at 90 min p.i. were treated with the indicated drugs or left untreated. (A) At 8 h p.i. (or 6.5 h p.i. for monensin) the cells were fixed and processed for FISH to detect segment 2 vRNA (red) and counterstained for NP protein (green). Small panels show *z* axis reconstructions. The scale bar indicates 16 μm. (B) Titers of supernatants were determined by plaque assay, and the results were plotted as the mean percentage ± SEM ($n \geq 3$) of the value from untreated cells. (C) Cell lysates were analyzed by SDS-PAGE and Western blotting, followed by densitometry for the indicated viral proteins. The means and ranges from two independent experiments are plotted.

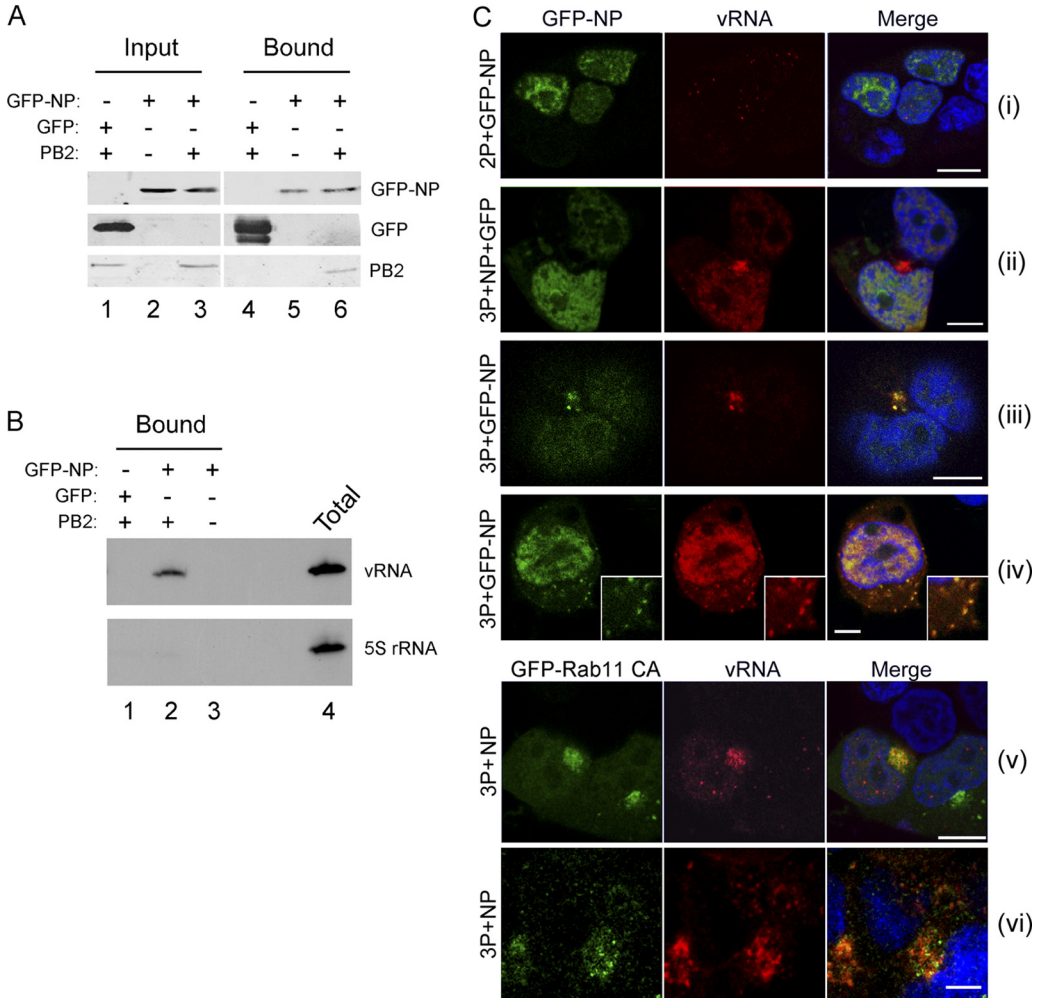

FIG. 5. Reconstitution of cytoplasmic RNP trafficking with GFP-tagged components. 293T cells were transfected with plasmids expressing segment 7 and 8 vRNAs and the minimal protein components of an influenza RNP, the three polymerase proteins (3P; or, as a nonfunctional control, two polymerase proteins lacking PB2 [2P]) and NP, as well as with plasmids expressing GFP-NP, GFP-Rab11 CA, or GFP as labeled. (A) At 48 h posttransfection, cells were lysed and analyzed by Western blotting for GFP and PB2 before (input) or after (bound) GFP-Trap affinity selection. (B) Bound RNA was analyzed by primer extension for segment 7 (vRNA) or 5S rRNA. A sample of infected cell RNA was analyzed in parallel as a marker (total). (C) At 24 h posttransfection, cells were fixed and stained for segment 7 vRNA by FISH. Nuclei were stained with 4′,6′-diamidino-2-phenylindole (DAPI). Scale bar, 5 μm.

introducing a large protein tag such as GFP into the viral genome, we turned to a plasmid-based minireplicon system in which the three polymerase proteins (3P), NP, and synthetic vRNAs are transcribed from cDNA (35, 38). Although our GFP-NP construct can functionally replace WT NP in the minireplicon setting (29), RNPs were reconstituted by transfecting a mixture of tagged and untagged NP to reduce the density of the GFP tag. Also, since the nuclear export of the viral genome requires both M1 and NEP proteins (8), we supplied segments 7 and 8 as vRNA templates, thus ensuring the expression of these proteins. To validate this system, we first tested for the successful reconstitution of RNPs by biochemical means. When lysates from transfected cells were incubated with GFP-affinity beads, PB2 coprecipitated with GFP-NP but not GFP (Fig. 5A, compare lanes 4 and 6), suggesting RNP formation. Confirming this, vRNA also was detectable in the bound fraction of lysates from cells containing 3P and GFP-NP, but not 3P and GFP or 2P (lacking PB2) and GFP-NP (Fig. 5B). We next examined the distribution of GFP-NP and vRNA in fixed cells. In control transfections lacking the PB2 subunit and thus a functional polymerase complex, the majority of GFP-NP was nuclear and relatively little signal was seen for segment 7 vRNA, with only a few nuclear foci of staining evident that potentially resulted from plasmid rather than viral transcription (Fig. 5C, image i). In contrast, when the full 3P-NP complex was present, bright nuclear and cytoplasmic vRNA staining was evident, with the latter often concentrating in a perinuclear structure as well as smaller, more dispersed foci throughout the cytoplasm (Fig. 5C, images ii to vi). When GFP-NP was included with the 3P-NP complex, the strong colocalization of the vRNA and GFP signal was seen both at the perinuclear region (image iii) and for the dispersed cytoplasmic puncta (image iv, inset). Similarly, when GFP-NP was replaced with a GFP-tagged con-

stitutively active (CA) Rab11 mutant, good colocalization was seen between vRNA and the fluorescent Rab11 protein both at the perinuclear region (image v) and for the smaller cytoplasmic granules (image vi). Thus, the RNP reconstitution assay successfully recapitulated the perinuclear accumulation of cytoplasmic vRNA seen in authentic viral infection, and furthermore it confirmed good cytoplasmic colocalization between GFP-NP and vRNA as well as between GFP-Rab11 CA and vRNA.

We next used this system to investigate the trafficking of viral RNPs in living cells by collecting time-lapse movies. Cells displaying the prominent perinuclear accumulation of GFP-NP (which thus likely contained successfully reconstituted RNPs) also showed the presence of many additional, smaller foci of NP in the cytoplasm (Fig. 6A). Many of the small GFP-NP foci remained approximately static (except for Brownian-type movement, which is defined here as random) during the observation period, but some exhibited the classic saltatory pattern of intermittent but rapid movement expected for microtubule-based transport. (see Movies S2 and S3 in the supplemental material; example tracks and selected frames are shown in Fig. 6A). Other particles showed more processive (defined as visible for at least five consecutive frames) but generally slower movement. When the speeds of multiple particles exhibiting the various classes of movement were measured, those that displayed random Brownian motion moved at an average of 0.12 ± 0.07 μm/s, while those exhibiting processive movement traveled at 0.25 ± 0.11 μm/s. In contrast, particles showing saltatory and/or bidirectional movement traveled at much faster speeds of up to nearly 3 μm/s with an average of 0.81 ± 0.40 μm/s (Fig. 6B and C). The large perinuclear accumulation remained mostly stationary, although its shape continually changed throughout observation and smaller particles could be seen to apparently both merge with and depart from it (see Movie S2 in the supplemental material).

To test the involvement of microtubules in RNP movement, transfected cells were treated with a panel of drugs that interfere with microtubule and/or vesicular transport and imaged up to 3 h later. From this, it was apparent that monensin treatment had a relatively slight (although statistically significant) effect on RNP movement (Fig. 6D), in contrast to its dramatic effect on vRNA trafficking in infected cells (Fig. 4). Under the shorter timescale of the live-cell imaging experiments, it is possible that monensin blocks the formation of new RE vesicles without disturbing the trafficking of preexisting ones (33). However, all drugs targeting microtubules caused a statistically significant, nearly complete loss of the fast, saltatory class of movement (Fig. 6D; an example of a nocodazole-treated cell is shown in Movie S4 in the supplemental material). These data further support the hypothesis that RNP cytoplasmic trafficking is mediated in part by the microtubule network.

Based on the observation that the number of cells displaying an obvious perinuclear accumulation of vRNA increased and then decreased during the infection cycle (Fig. 1C), we hypothesized that RNPs localized there first before distributing to the cell periphery to be assembled into budding virions. Therefore, we used fluorescence recovery after photobleaching (FRAP) to examine whether GFP-tagged NP in the perinuclear compartment dynamically exchanges. A bleach area large enough to cover the entire perinuclear compartment was defined (Fig. 7A) to ensure that FRAP recovery represented the exchange of GFP-NP with the cytoplasm rather than an internal rearrangement of protein in the compartment or movement in the *z* axis. Relatively slow but consistent recovery of fluorescence within the perinuclear body was observed, on average to $10.8\% \pm 1.3\%$ of the initial value during a period of 85 s (Fig. 7A to C; also see Movie S5 in the supplemental material), indicating measurable but limited exchange with the perinuclear compartment during the period of a minute or so. Thus, the perinuclear compartment is not static, but neither is there rapid exchange with GFP-NP in the cytoplasm; this finding is compatible with the directed transport of RNPs rather than free diffusion.

Since cytoplasmic NP and vRNA colocalized well with endogenous and CA forms of Rab11 in fixed cells (10) (Fig. 3 and 5), we tested whether this extended to living cells by transfecting cells with plasmids to reconstitute cytoplasmic GFP-tagged RNPs as before and additionally with an otherwise WT RFP-tagged Rab11. An excellent degree of colocalization between cytoplasmic puncta of GFP-NP and RFP-Rab11 was seen (Fig. 6E). Furthermore, time-lapse imaging showed that many of the structures double labeled with the two fluorophores displayed the characteristic rapid, saltatory movement in which particles sometimes reversed direction (see Movie S6 in the supplemental material).

We next tested whether the colocalization and cotrafficking of NP, vRNA, and Rab11 in cells reflected an interaction that could be detected biochemically. Cells were transfected with GFP-Rab11 CA or, as negative controls, with GFP-Rab11 DN, GFP-Rab8 CA, or GFP alone. GFP-Rab11 DN does not colocalize with NP in infected cells, while Rab8 is not known to play a role in the influenza virus life cycle (10). Following virus superinfection, cell lysates were prepared and analyzed by Western blotting for GFP and selected viral proteins before or after fractionation over GFP-affinity beads. The P proteins, NP, M1, M2, and various GFP polypeptides were detected as expected in the cell lysates (Fig. 8A, lanes 1 to 5). GFP-containing polypeptides also were retained as expected on the anti-GFP beads (lanes 6 to 10). Only trace quantities of M1 or M2 were detected in any of the bound fractions. However, NP and the P proteins were readily detectable in the sample containing GFP-Rab11 CA, while only background amounts were seen in samples containing GFP-Rab11 DN or GFP-Rab8 CA proteins (Fig. 8A, compare lane 7 to lanes 6, 9, and 10). The quantification of the amounts of the viral proteins bound under various conditions from replicate experiments showed that the protein components of the viral RNP were consistently precipitated by GFP-Rab11 CA at around 10 times the level obtained with GFP alone or with GFP Rab11 DN, Rab8 CA, or Rab4 CA (Fig. 8B), strongly suggesting that RNPs interact with the GTP-bound form of Rab11. In confirmation of this, vRNA also was directly detected in samples affinity purified with GFP-Rab11 CA but not the other GFP polypeptides (Fig. 8C). To determine which component of the influenza virus RNP interacts with GTP-bound Rab11, we cotransfected the individual RNP subunits with GFP-Rab11 CA or GFP and performed GFP-affinity pulldowns. No detectable amounts of NP, PB1, or PA were precipitated under these conditions despite their presence in the starting cell lysates, whereas PB2 was specifi-

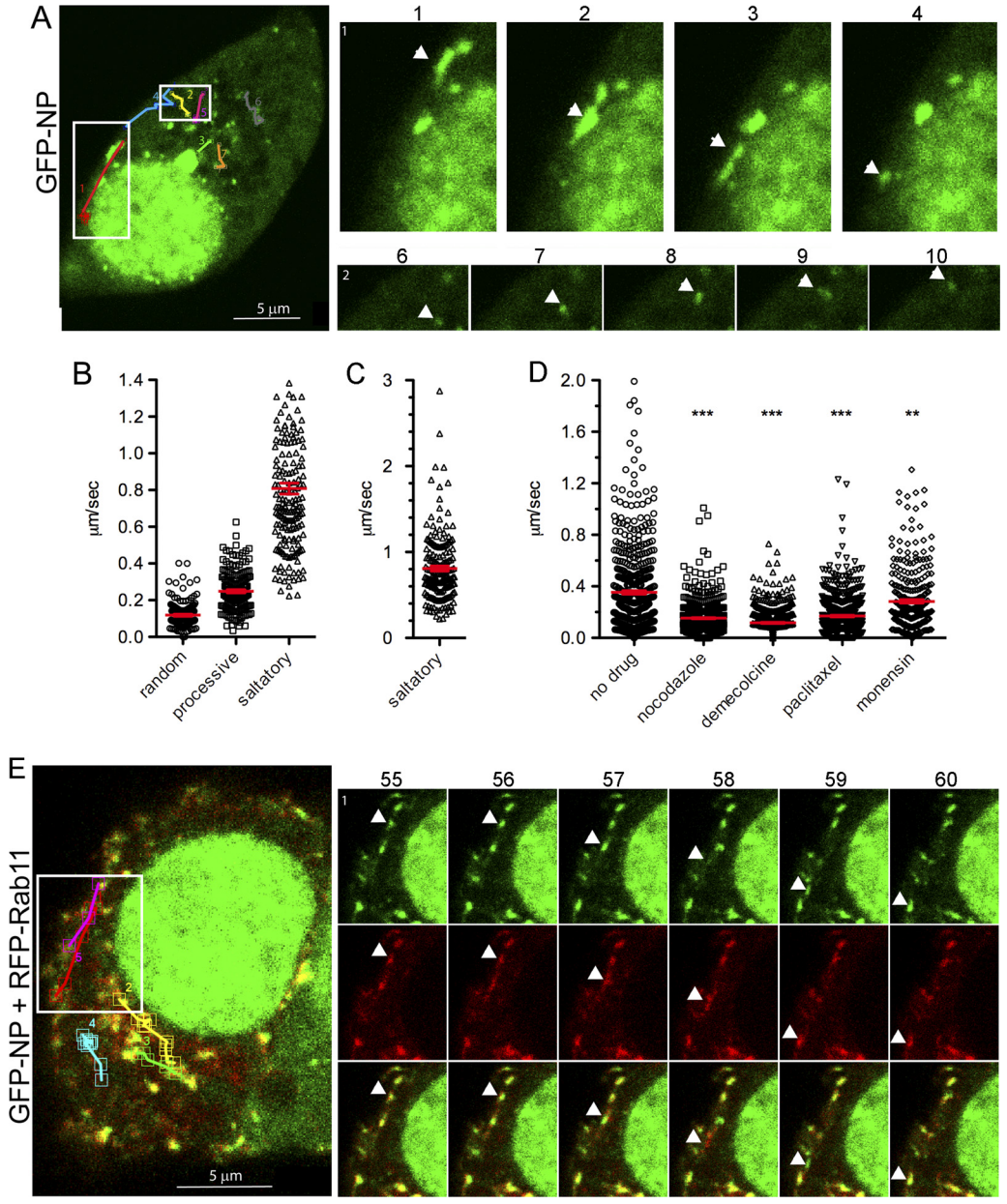

FIG. 6. Live-cell trafficking of GFP-NP and RFP-Rab11. 293T cells were transfected with plasmids to reconstitute viral RNPs containing segments 7 and 8 plus either GFP-NP (A to D) or GFP-NP and RFP-Rab11 (E) before imaging under time-lapse conditions (approximately every 4 s) at 24 h posttransfection. (A and E) Single images at time zero are shown in the large panels with the tracks of selected particles indicated, while individual frames with single moving particles highlighted with arrowheads are shown in the small panels. For example, track 1 shows saltatory class movement followed by Brownian-type movement, and track 2 is classified as processive-type movement. Note that in panel E the apparent spatial separation of red and green images of fast-moving particles is likely to be an artifact resulting from the time taken for the microscope to switch between channels. (B to D) Particle speeds were measured between consecutive frames of time-lapse movies using ImageJ. Each data point represents one measurement between consecutive frames. (B and C) Values from untreated cells were grouped according to whether the particles demonstrated nondirectional Brownian-type motion (random), steady processive motion, or saltatory/bidirectional motion during the course of individual movies. A partial data set of saltatory movement, excluding a small number of very fast moving particles, is plotted in panel B to avoid the visual compression of the lower-value data points, while the full data set is plotted separately in panel C. A total of 98 particles from 16 cells from 10 independent transfections were analyzed. (D) Values from cells treated with the indicated drugs or left untreated (pooled data from panel B) are plotted. A minimum of 54 particles from between 7 and 16 cells from two to three independent experiments were analyzed, focusing on the fastest moving particles within the cells. Red bars indicate the means ± SEM. Asterisks indicate the outcome of statistical tests (nonparametric, two-tailed Mann-Whitney *t* test) for differences between the treated and untreated samples. ***, $P < 0.001$; **, $P < 0.01$. Also see Movies S2 to 4 and 6 in the supplemental material.

cally bound by GFP-Rab11 CA but not by GFP alone (Fig. 8D). When replicate experiments were quantified, levels of PB2 bound by GFP-Rab11 were around 6-fold higher than those precipitated by GFP alone, while the amounts of PB1, PA, and NP were similar for both ligands (Fig. 8E). These data are consistent with the microscopy data showing the colocalization of viral RNPs with WT or CA forms of Rab11 (Fig. 3, 5, and 6) but not the DN form (10) and support the

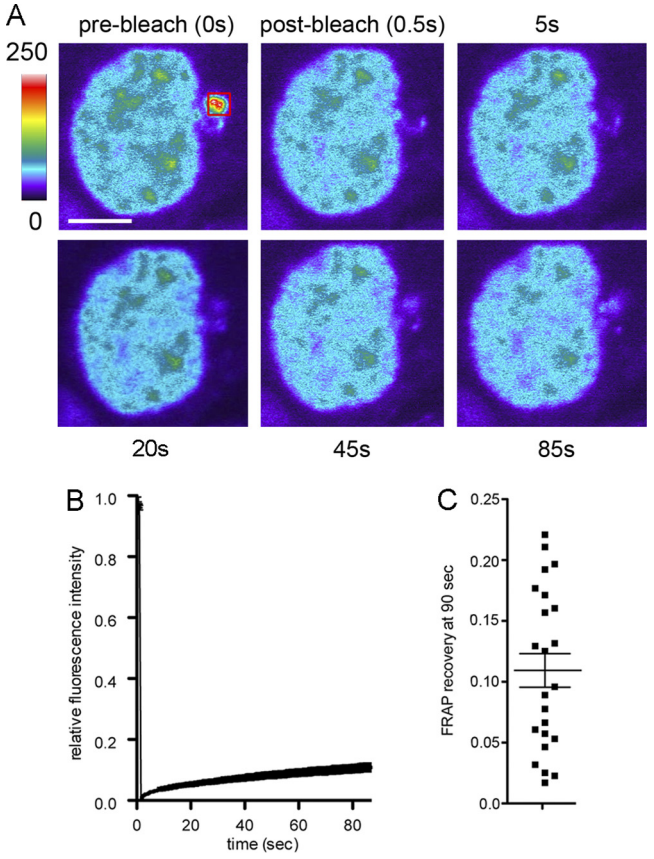

FIG. 7. FRAP analysis of the perinuclear compartment. RNPs were reconstituted in 293T cells as described in the legend to Fig. 5, and perinuclear areas of fluorescence were subjected to FRAP analysis. (A) Representative images from one cell (colored according to fluorescence intensity in arbitrary units) are shown. The scale bar is 5 μm, and the red square denotes the bleach area. (B) The mean ± SEM ($n = 24$) recovery curve is plotted. (C) The fraction of initial fluorescence recovered at 85 s after the bleaching of individual cells is plotted. Horizontal lines indicate the means ± SEM. Also see Movie S5 in the supplemental material.

hypothesis that RNPs traffic via an Rab11-dependent pathway potentially mediated by an interaction with the PB2 subunit of the polymerase.

We recently showed that the siRNA-mediated depletion of Rab11 in 293T cells caused defects in influenza A virus budding without obvious alterations to NP localization (10). However, we did not examine vRNA localization directly, and 293T cells have a small cytoplasmic volume, which may have masked more subtle effects on NP trafficking. We therefore examined the effect the loss of Rab11 had on vRNA distribution in A549 cells, which have a much larger cytoplasm/nuclear ratio. Cells were depleted of Rab11a and Rab11b isoforms by siRNA treatment as before (10); Western blot analysis of Rab11a and selected viral proteins confirmed the effective knockdown of Rab11 without major effect on viral gene expression (Fig. 9A). When replicate experiments were quantified, an average depletion of around 90% was obtained. We then examined the effect this had on RNP localization across a time course of virus infection. In cells treated with control siRNA oligonucleotides, vRNA and NP displayed time-dependent changes in localization similar to those seen in other cell types: early nuclear accumulation (with NP but not vRNA, tending to concentrate toward the nuclear periphery), followed by increasing cytoplasmic accumulation at later time points (Fig. 9B). The cytoplasmic phase of RNP localization included the initial accumulation of vRNA at a perinuclear site (Fig. 9B, 7 h, arrowheads), which in some cells apparently was associated with filamentous or tubular structures (Fig. 9B, 7 h, inset). At later time points, the perinuclear vRNA staining was lost, being replaced by many large (≥1-μm) aggregates dispersed throughout the cytoplasm, which mostly double stained for both vRNA and NP (Fig. 9B, 10- and 16-h time points, and C). In cells depleted of Rab11, vRNA still accumulated in the nucleus at an early time point and was successfully exported to the cytoplasm thereafter (Fig. 9D). However, the pattern of RNP localization in the cytoplasm was considerably altered, as the initial perinuclear accumulation and the subsequent large cytoplasmic structures were absent, being replaced instead with a much more dispersed, finer-grained pattern of staining (Fig. 9C and D). Thus, the depletion of Rab11 leads to altered vRNA trafficking in A549 cells.

Finally, we asked whether NP and Rab11 interacted in infected A549 cells, since the majority of our previous data came from 293T cells and overexpressed Rab11. Attempts to detect an interaction between endogenous Rab11 and RNPs by pull-down assay were unsuccessful (from A549 or 293T cells; data not shown). We therefore turned to the Duolink PLA *in situ* cell-based fluorescence proximity assay, in which closely apposed (~40 nm or less) primary antibodies are detected by the amplification of intermolecular ligation events of oligonucleotides covalently attached to secondary antibodies (54). When cells were double stained by this procedure for NP and either Rab11 or Rab4 (as a negative control), the numbers of detected events were around 70-fold higher in infected cells than in mock-infected cells for Rab11 but were only around 15-fold higher for Rab4 (Fig. 9E). In cells first depleted of Rab11, however, levels of signal from Rab11 and NP but not Rab4 and NP were drastically reduced, indicating the specificity of the reaction. Thus, while not proving a physical interaction, NP and Rab11 normally are in close proximity during infection.

To provide information on where the NP-Rab11 interaction occurred in A549 cells, we performed conventional indirect immunofluorescence. In uninfected A549 cells, endogenous Rab11 was difficult to detect by this method, producing faint punctate staining throughout the cytoplasm as well as the more distinct labeling of a perinuclear structure likely to be the RE (Fig. 10). Unexpectedly, Rab11 staining was markedly more intense in infected cells. At 7 h p.i., brighter punctate staining throughout the cytoplasm was apparent, and in many cells, there was prominent perinuclear staining with obvious colocalization with NP (Fig. 10, arrows). Late in infection, large cytoplasmic aggregates of Rab11 appeared that again colocalized strongly with NP (Fig. 10, 16 h p.i.). The virus-induced increase in the intensity of Rab11 staining did not result from increased amounts of the protein, as judged by Western blot analysis (Fig. 9A), but it was not artifactual cross-reactivity with another antigen, since infected cells depleted of Rab11 by siRNA treatment displayed very low levels of staining (Fig. 10). One possibility is that the more concentrated protein facilitates detection, although an infection-dependent unmasking of the

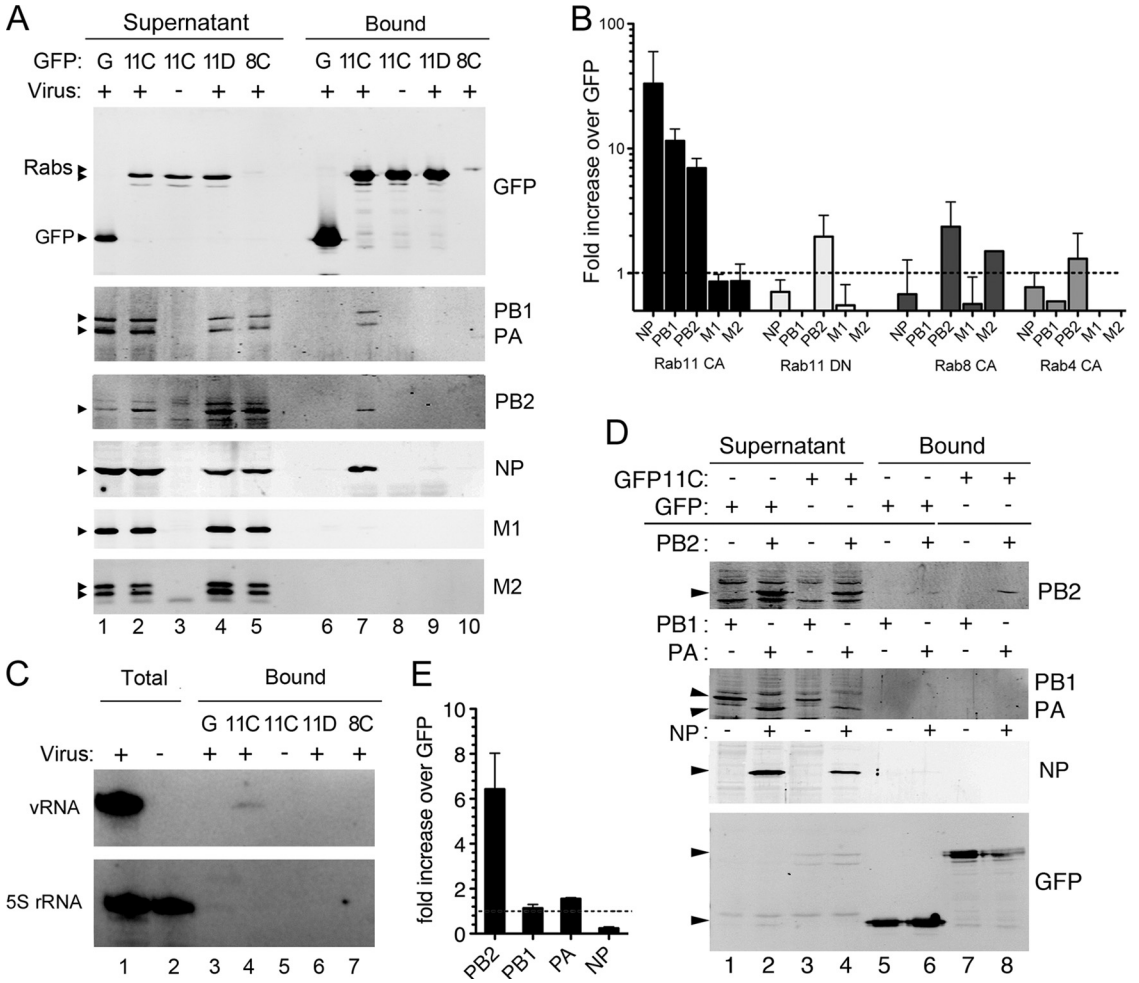

FIG. 8. Biochemical association of RNPs and Rab11. (A to C) 293T cells were transfected with plasmids expressing GFP alone or the indicated GFP-Rab proteins (11C, Rab11 CA; 11D, Rab11 DN; 8C, Rab8 CA) and infected (or mock infected) 48 h later with PR8 virus. (A) Cell lysates prepared at 6 h p.i. were analyzed by Western blotting for the indicated polypeptides after GFP-Trap affinity selection into supernatant and bound fractions. Sample loading is such that the supernatants are equivalent to 1/10 the bound fractions. (B) Bound protein was quantified from replicate experiments and is plotted as the mean ± SEM fold increase relative to levels for the GFP control. (C) RNA was analyzed by primer extension for segment 7 vRNA and 5S rRNA before (total) or after GFP-TRAP selection. (D and E) 293T cells were transfected with the indicated plasmids and analyzed by GFP-TRAP affinity selection followed by Western blotting as for panels A and B.

Rab11 C-terminal sequence recognized by the antibody also is possible. The depletion of Rab11 did, however, again lead to the altered cytoplasmic distribution of NP as previously observed for vRNA (Fig. 9D and 10). Overall, therefore, RNPs colocalized with Rab11 in A549 cells, and the loss of Rab11 altered their pattern of cytoplasmic localization. This supports the hypothesis that the cytoplasmic trafficking of the influenza virus genome involves Rab11.

DISCUSSION

Our aim was to better define the trafficking mechanism(s) responsible for the transport of the influenza A virus genome from the nuclear to plasma membranes. Using a combination of static and live-cell imaging techniques, we provide evidence for two distinct patterns of vRNA localization in the cytoplasm (perinuclear and dispersed cytoplasmic granules), as well as evidence that RNPs traffic in part using the microtubule-based vesicular transport system, and that the adaptor linking viral and cellular components for this process is Rab11. We interpret our data as supporting a two-step model for the cytoplasmic trafficking of the viral genome, in which after leaving the nucleus, RNPs first accumulate at the pericentriolar recycling endosomal compartment through an interaction with Rab11 and then piggyback onto the microtubule network via vesicles destined for the cell periphery (Fig. 11).

The perinuclear accumulation of NP and vRNA has been noted before (10, 28, 34). Here, we extend this observation by showing that it is a time-dependent phenomenon occurring midway through infection, that it can be seen in living cells, and that it occurs with several strains of virus in different cell types, making it likely that it reflects an important feature of the viral life cycle. We also identify the location as the pericentriolar recycling endosomal compartment. We base this on the failure of vRNA to meaningfully colocalize with other cellular vesicular markers found in this region of the cell, including *cis* and

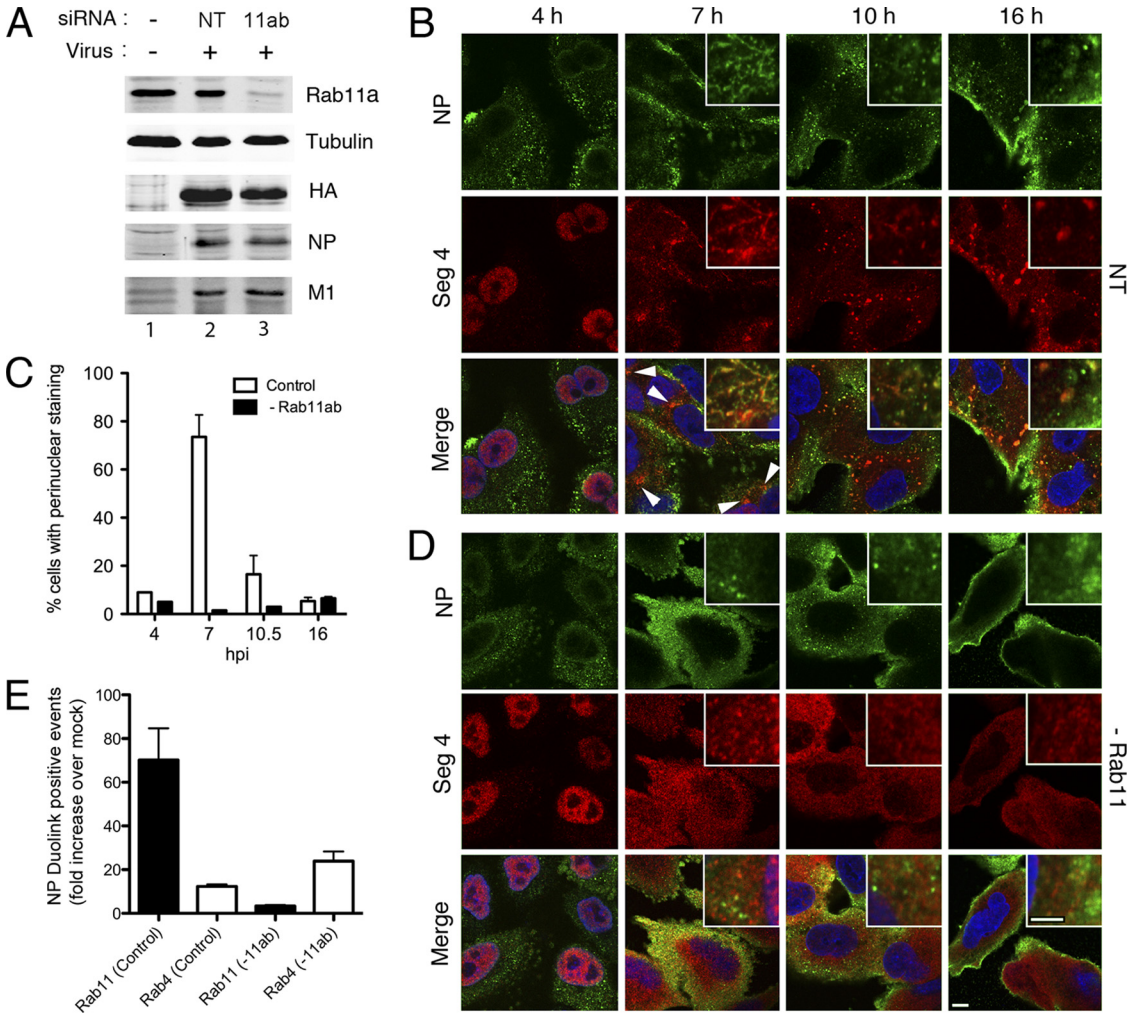

FIG. 9. Effect of siRNA depletion of Rab11 on RNP localization. A549 cells were transfected or mock transfected (−) with siRNAs against Rab11a and Rab11b (Rab11) or with a nontargeting control (NT) and infected or mock infected 3 days later with PR8 virus as indicated. (A) At 16 h p.i., cell lysates were analyzed by Western blotting for the indicated proteins. (B to D) A549 cells were treated with nontargeting (NT) or (D) with siRNAs against Rab11a and Rab11b, infected 3 days later with PR8 virus, fixed at the indicated times p.i., and stained for segment 4 vRNA and NP. Merged-image panels also show 4′,6′-diamidino-2-phenylindole (DAPI) staining for nuclei. All images were collected at equal microscope settings, but the 4-h panels are shown at increased brightness. Scale bars, 5 μm. (C) The percentage (means ± SE) of cells showing an obvious perinuclear accumulation of vRNA was scored at various times p.i. (E) Cells were fixed and analyzed for NP proximity to the indicated Rab proteins by a Duolink PLA fluorescence proximity assay. The number of fluorescent spots per nuclei (>360 cells) of single optical sections were counted and are presented as the mean ± SEM (n = 2 to 3 independent experiments) increase above levels for similarly stained mock-infected cells.

trans compartments of the Golgi network, as well as markers for early endosomes or aggresomes (data not shown). Evidence in favor of this is that vRNA and Rab11a overlap was significant, while GFP-NP-tagged RNPs also colocalized near the MTOC with transferrin (data not shown). Both Rab11a and transferrin serve as markers for the pericentriolar RE compartment (20, 43, 56). The apparently tubular localization pattern seen for vRNA in a subset of A549 cells also is consistent with localization at the RE (25). However, we disagree with previous conclusions that perinuclear RNPs colocalized with markers for the TGN (28, 34).

We propose that vRNAs accumulate at the pericentriolar RE first before moving to the periphery of the cell. This aspect of the model is based on the observations that vRNA localization here is seen soon after the onset of genome replication and export and that it tends to fade later in infection, suggesting a dynamic rather than static association. Further supporting this, the observation of GFP-tagged NP particle movement in living cells was consistent with the movement of RNPs both into and out of the perinuclear body during relatively short time scales. It also is supported by the persistence of vRNA staining in the perinuclear region after vesicular transport in infected cells was blocked by treatment with monensin. The model also is consistent with the known directionality of Rab11 in directing vesicular trafficking from the RE to the plasma membrane (43, 56, 59).

We hypothesize that an interaction between PB2 and Rab11 recruits the viral genome to the pericentriolar RE

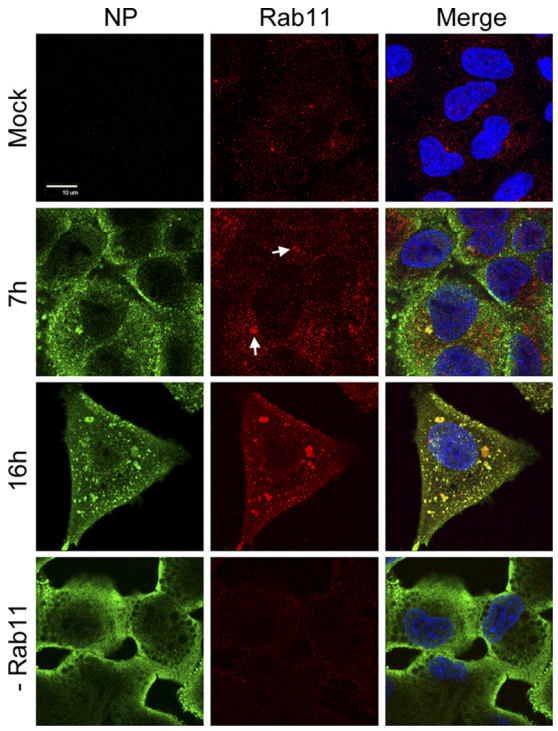

FIG. 10. Colocalization of Rab11 and NP in A549 cells. Cells were infected or mock infected with PR8 virus, fixed at 16 h p.i., and stained for NP and Rab11. Scale bar, 10 μm.

based on the finding that all components of an RNP can be specifically coprecipitated by the GTP-bound form of Rab11 from infected cells but only PB2 as an individual protein, and that in the absence of normal levels of Rab11 RNPs do not concentrate at the perinuclear site. Also, their cytoplasmic localization in general is altered. The simplest hypothesis is a direct protein-protein interaction between PB2 and Rab11, but at present we cannot rule out bridging interactions with other cellular proteins, such as a Rab11-family interacting protein.

In a refinement of a recent proposal that RNP trafficking involves the vesicular transport system (28), we also postulate that RNP transport to the cell periphery is at least partly based on an attachment to Rab11-positive vesicles that move via microtubules, which is consistent with the known transport of such cellular cargo (3, 7, 13). In evidence of microtubule-based movement of RNPs, the speeds and saltatory character exhibited by many GFP-NP particles in time-lapse movies of living cells are diagnostic as well as consistent with the values measured for the movement of intracellular enveloped vaccinia virus on microtubules (44, 57). We also point to the disruption of normal vRNA localization seen after treatment with specific inhibitors of the microtubule network. Similar perturbations of cytoplasmic NP localization after treatment with inhibitors of microtubule function have been reported previously (34). The apparent misdirection of vRNA to the lateral membranes of MDCK cells after nocodazole treatment also is consistent with a study that found a loss of polarity in virus budding under similar circumstances (45). It is worth noting that nocodazole treatment has been shown previously to disperse Rab11-positive vesicles, resulting in an accumulation at the lateral membranes (3, 13). Evidence for RNP trafficking piggybacking on vesicles is less direct, as at present we cannot formally exclude a mechanism in which RNPs are targeted to microtubules without an intervening lipid structure. However, we think this hypothesis is reasonable given the extensive colocalization between NP, vRNA, and both WT and CA forms of Rab11 and the fact that the GTP-bound form of Rab11 would be expected to be membrane bound. It also is consistent with the observa-

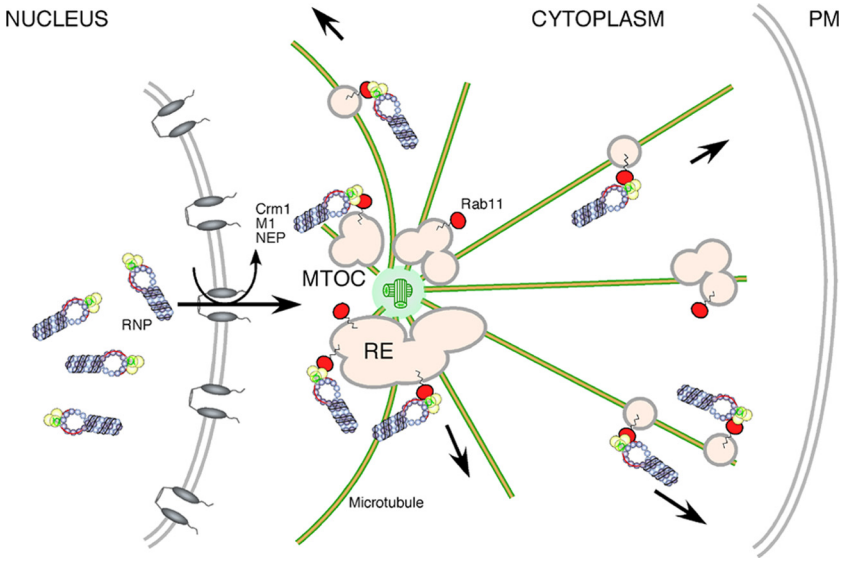

FIG. 11. Cartoon model for influenza virus RNP trafficking. RNPs are replicated within the nucleus and exported via cellular Crm1 and viral NEP and M1 proteins. They initially concentrate at the pericentriolar recycling endosome (RE) adjacent to the microtubule organizing center (MTOC) through interactions with Rab11. Subsequently, they traffic along the microtubule network toward the cell periphery and plasma membrane (PM) on Rab11-positive cargo vesicles.

tion that monensin treatment throughout infection inhibits vRNA movement away from the RE.

We would not argue that all RNP transport occurs via the model just described. While we measured saltatory movement consistent with microtubule-based trafficking for some RNP particles, others exhibited diffusional-type movement, similarly to that previously observed for microinjected RNPs (6). Other GFP-NP particles exhibited short-range processive movement with an average speed of around 0.2 μm/s, which is consistent with actin-based motility (44). These observations, together with the relatively minor effects of microtubule-disrupting drugs on virus replication and the diffuse localization of vRNA in Rab11-depleted cells, make it plausible that redundant mechanisms apply in transporting vRNPs to the plasma membrane. We hypothesize that microtubules are required for the efficient long-range delivery of RNPs, while other modes of transport (i.e., diffusion or along microfilaments) also operate, potentially over shorter ranges and/or in different areas of the cell. A degree of functional redundancy may explain the relatively minor effects cytoskeletal poisons have on the overall titer of virus replication in cell culture.

Our model for vRNA trafficking may have parallels with certain other viruses. Notably, the capsid assembly of certain retroviruses has been proposed to take place at the pericentriolar RE (1), and this region of the cell also may be used as a way point by several large DNA viruses (60). Most notably, however, our findings are strikingly similar to those recently reported for the nonsegmented negative-sense Sendai virus, in which the colocalization of viral RNPs and Rab11a as well as the microtubule-based movement of the RNPs was shown (14).

Previous work in our laboratory (10) showed that Rab11 was required for virus budding. However, the question of whether Rab11 was directly involved in mediating membrane scission or indirectly linked (by transporting a viral or cellular factor essential for pinching off) was not resolved in our earlier work. We did not observe a notable NP-trafficking defect in Rab11-depleted 293T cells (10), in contrast to the greatly altered distribution of NP and vRNA seen in depleted A549 cells here. A549 cells, as human lung cells with considerable cytoplasmic volumes, represent a more authentic model to study viral trafficking. The discrepancies seen in some circumstances between the indirect immunofluorescent staining of NP and FISH staining of vRNA (e.g., Fig. 1B, 4-h time points, and Fig. 9, 4- and 16-h time points) also raise the possibility of separate pools of free NP in the cytoplasm and nucleus. Nevertheless, the role of Rab11 in influenza RNP trafficking presented here is consistent with the theory that Rab11 is indirectly involved in viral budding. One possibility is that Rab11 also is required for the efficient delivery of M2 to the apical plasma membrane (48). However, the possibility that the trafficking of the viral genome is specifically required to allow efficient virus assembly and/or budding is an attractive hypothesis and is one that represents an area of future research.

ACKNOWLEDGMENTS

We thank Colin Crump, Folma Buss, Stephen Ferguson, Janet Daly, and Miguel Seabra for the gift of reagents and Fumitaka Momose for helpful discussion and sharing unpublished data.

This work was supported by a grant from the MRC (no. G0700815) to P.D. E.A.B. is supported by a studentship from the Gates Cambridge Trust. E.K.C.R., A.F., and R.M. are supported by studentships from the Wellcome Trust.

REFERENCES

1. **Afonso, P. V., A. Zamborlini, A. Saib, and R. Mahieux.** 2007. Centrosome and retroviruses: the dangerous liaisons. Retrovirology **4:**27.
2. **Amorim, M. J., E. K. Read, R. M. Dalton, L. Medcalf, and P. Digard.** 2007. Nuclear export of influenza A virus mRNAs requires ongoing RNA polymerase II activity. Traffic **8:**1–11.
3. **Apodaca, G., L. A. Katz, and K. E. Mostov.** 1994. Receptor-mediated transcytosis of IgA in MDCK cells is via apical recycling endosomes. J. Cell Biol. **125:**67–86.
4. **Arcangeletti, M. C., et al.** 1997. Modification of cytoskeleton and prosome networks in relation to protein synthesis in influenza A virus-infected LLC-MK2 cells. Virus Res. **51:**19–34.
5. **Avalos, R. T., Z. Yu, and D. P. Nayak.** 1997. Association of influenza virus NP and M1 proteins with cellular cytoskeletal elements in influenza virus-infected cells. J. Virol. **71:**2947–2958.
6. **Babcock, H. P., C. Chen, and X. Zhuang.** 2004. Using single-particle tracking to study nuclear trafficking of viral genes. Biophys. J. **87:**2749–2758.
7. **Balasubramanian, N., D. W. Scott, J. D. Castle, J. E. Casanova, and M. A. Schwartz.** 2007. Arf6 and microtubules in adhesion-dependent trafficking of lipid rafts. Nat. Cell Biol. **9:**1381–1391.
8. **Boulo, S., H. Akarsu, R. W. Ruigrok, and F. Baudin.** 2007. Nuclear traffic of influenza virus proteins and ribonucleoprotein complexes. Virus Res. **124:**12–21.
9. **Breitenfeld, P. M., and W. Schafer.** 1957. The formation of fowl plague virus antigens in infected cells, as studied with fluorescent antibodies. Virology **4:**328–345.
10. **Bruce, E. A., P. Digard, and A. D. Stuart.** 2010. The Rab11 pathway is required for influenza A virus budding and filament formation. J. Virol. **84:**5848–5859.
11. **Bruce, E. A., et al.** 2009. Budding of filamentous and non-filamentous influenza A virus occurs via a VPS4 and VPS28-independent pathway. Virology **390:**268–278.
12. **Carrasco, M., M. J. Amorim, and P. Digard.** 2004. Lipid raft-dependent targeting of the influenza A virus nucleoprotein to the apical plasma membrane. Traffic **5:**979–992.
13. **Casanova, J. E., et al.** 1999. Association of Rab25 and Rab11a with the apical recycling system of polarized Madin-Darby canine kidney cells. Mol. Biol. Cell **10:**47–61.
14. **Chambers, R., and T. Takimoto.** 2010. Trafficking of Sendai virus nucleocapsids is mediated by intracellular vesicles. PLoS One **5:**e10994.
15. **Chen, B. J., G. P. Leser, E. Morita, and R. A. Lamb.** 2007. Influenza virus hemagglutinin and neuraminidase, but not the matrix protein, are required for assembly and budding of plasmid-derived virus-like particles. J. Virol. **81:**7111–7123.
16. **Dale, L. B., J. L. Seachrist, A. V. Babwah, and S. S. Ferguson.** 2004. Regulation of angiotensin II type 1A receptor intracellular retention, degradation, and recycling by Rab5, Rab7, and Rab11 GTPases. J. Biol. Chem. **279:**13110–13118.
17. **de Wit, E., et al.** 2004. Efficient generation and growth of influenza virus A/PR/8/34 from eight cDNA fragments. Virus Res. **103:**155–161.
18. **Digard, P., V. C. Blok, and S. C. Inglis.** 1989. Complex formation between influenza virus polymerase proteins expressed in Xenopus oocytes. Virology **171:**162–169.
19. **Digard, P., et al.** 1999. Modulation of nuclear localization of the influenza virus nucleoprotein through interaction with actin filaments. J. Virol. **73:**2222–2231.
20. **Dunn, K. W., T. E. McGraw, and F. R. Maxfield.** 1989. Iterative fractionation of recycling receptors from lysosomally destined ligands in an early sorting endosome. J. Cell Biol. **109:**3303–3314.
21. **Elton, D., et al.** 2001. Interaction of the influenza virus nucleoprotein with the cellular CRM1-mediated nuclear export pathway. J. Virol. **75:**408–419.
22. **Griffin, J. A., and R. W. Compans.** 1979. Effect of cytochalasin B on the maturation of enveloped viruses. J. Exp. Med. **150:**379–391.
23. **Harman, A., H. Browne, and T. Minson.** 2002. The transmembrane domain and cytoplasmic tail of herpes simplex virus type 1 glycoprotein H play a role in membrane fusion. J. Virol. **76:**10708–10716.
24. **Hayman, A., et al.** 2007. NS1 proteins of avian influenza A viruses can act as antagonists of the human alpha/beta interferon response. J. Virol. **81:**2318–2327.
25. **Hopkins, C. R., A. Gibson, M. Shipman, D. K. Strickland, and I. S. Trowbridge.** 1994. In migrating fibroblasts, recycling receptors are concentrated in narrow tubules in the pericentriolar area, and then routed to the plasma membrane of the leading lamella. J. Cell Biol. **125:**1265–1274.
26. **Hutchinson, E. C., M. D. Curran, E. K. Read, J. R. Gog, and P. Digard.** 2008. Mutational analysis of cis-acting RNA signals in segment 7 of influenza A virus. J. Virol. **82:**11869–11879.
27. **Hutchinson, E. C., J. C. von Kirchbach, J. R. Gog, and P. Digard.** 2010. Genome packaging in influenza A virus. J. Gen. Virol. **91:**313–328.
28. **Jo, S., et al.** 2010. Involvement of vesicular trafficking system in membrane

targeting of the progeny influenza virus genome. Microbes Infect. **12:**1079–1084.
29. **Loucaides, E. M., et al.** 2009. Nuclear dynamics of influenza A virus ribonucleoproteins revealed by live-cell imaging studies. Virology **394:**154–163.
30. **Martin, K., and A. Helenius.** 1991. Nuclear transport of influenza virus ribonucleoproteins: the viral matrix protein (M1) promotes export and inhibits import. Cell **67:**117–130.
31. **Mayer, D., et al.** 2007. Identification of cellular interaction partners of the influenza virus ribonucleoprotein complex and polymerase complex using proteomic-based approaches. J. Proteome Res. **6:**672–682.
32. **Meijering, E., et al.** 2004. Design and validation of a tool for neurite tracing and analysis in fluorescence microscopy images. Cytometry A **58:**167–176.
33. **Mollenhauer, H. H., D. J. Morre, and L. D. Rowe.** 1990. Alteration of intracellular traffic by monensin; mechanism, specificity and relationship to toxicity. Biochim. Biophys. Acta **1031:**225–246.
34. **Momose, F., Y. Kikuchi, K. Komase, and Y. Morikawa.** 2007. Visualization of microtubule-mediated transport of influenza viral progeny ribonucleoprotein. Microbes Infect. **9:**1422–1433.
35. **Mullin, A. E., R. M. Dalton, M. J. Amorim, D. Elton, and P. Digard.** 2004. Increased amounts of the influenza virus nucleoprotein do not promote higher levels of viral genome replication. J. Gen. Virol. **85:**3689–3698.
36. **Nayak, D. P., R. A. Balogun, H. Yamada, Z. H. Zhou, and S. Barman.** 2009. Influenza virus morphogenesis and budding. Virus Res. **143:**147–161.
37. **Noton, S. L., et al.** 2007. Identification of the domains of the influenza A virus M1 matrix protein required for NP binding, oligomerization and incorporation into virions. J. Gen. Virol. **88:**2280–2290.
38. **Pleschka, S., et al.** 1996. A plasmid-based reverse genetics system for influenza A virus. J. Virol. **70:**4188–4192.
39. **Poole, E., D. Elton, L. Medcalf, and P. Digard.** 2004. Functional domains of the influenza A virus PB2 protein: identification of NP- and PB1-binding sites. Virology **321:**120–133.
40. **Portela, A., and P. Digard.** 2002. The influenza virus nucleoprotein: a multifunctional RNA-binding protein pivotal to virus replication. J. Gen. Virol. **83:**723–734.
41. **Radtke, K., K. Dohner, and B. Sodeik.** 2006. Viral interactions with the cytoskeleton: a hitchhiker's guide to the cell. Cell Microbiol. **8:**387–400.
42. **Read, E. K., and P. Digard.** 2010. Individual influenza A virus mRNAs show differential dependence on cellular NXF1/TAP for their nuclear export. J. Gen. Virol. **91:**1290–1301.
43. **Ren, M., et al.** 1998. Hydrolysis of GTP on rab11 is required for the direct delivery of transferrin from the pericentriolar recycling compartment to the cell surface but not from sorting endosomes. Proc. Natl. Acad. Sci. U. S. A. **95:**6187–6192.
44. **Rietdorf, J., et al.** 2001. Kinesin-dependent movement on microtubules precedes actin-based motility of vaccinia virus. Nat. Cell Biol. **3:**992–1000.
45. **Rindler, M. J., I. E. Ivanov, and D. D. Sabatini.** 1987. Microtubule-acting drugs lead to the nonpolarized delivery of the influenza hemagglutinin to the cell surface of polarized Madin-Darby canine kidney cells. J. Cell Biol. **104:**231–241.
46. **Robb, N. C., M. Smith, F. T. Vreede, and E. Fodor.** 2009. NS2/NEP protein regulates transcription and replication of the influenza virus RNA genome. J. Gen. Virol. **90:**1398–1407.
47. **Roberts, P. C., and R. W. Compans.** 1998. Host cell dependence of viral morphology. Proc. Natl. Acad. Sci. U. S. A. **95:**5746–5751.
48. **Rossman, J. S., X. Jing, G. P. Leser, and R. A. Lamb.** 2010. Influenza virus M2 protein mediates ESCRT-independent membrane scission. Cell **142:**902–913.
49. **Sahlender, D. A., et al.** 2005. Optineurin links myosin VI to the Golgi complex and is involved in Golgi organization and exocytosis. J. Cell Biol. **169:**285–295.
50. **Salas, P. J., et al.** 1986. Microtubules and actin filaments are not critically involved in the biogenesis of epithelial cell surface polarity. J. Cell Biol. **102:**1853–1867.
51. **Seachrist, J. L., P. H. Anborgh, and S. S. Ferguson.** 2000. Beta 2-adrenergic receptor internalization, endosomal sorting, and plasma membrane recycling are regulated by rab GTPases. J. Biol. Chem. **275:**27221–27228.
52. **Shaw, M. L., K. L. Stone, C. M. Colangelo, E. E. Gulcicek, and P. Palese.** 2008. Cellular proteins in influenza virus particles. PLoS Pathog. **4:**e1000085.
53. **Simpson-Holley, M., et al.** 2002. A functional link between the actin cytoskeleton and lipid rafts during budding of filamentous influenza virions. Virology **301:**212–225.
54. **Söderberg, O., et al.** 2006. Direct observation of individual endogenous protein complexes in situ by proximity ligation. Nat. Methods **3:**995–1000.
55. **Taubenberger, J. K., and J. C. Kash.** 2010. Influenza virus evolution, host adaptation, and pandemic formation. Cell Host Microbe **7:**440–451.
56. **Ullrich, O., S. Reinsch, S. Urbe, M. Zerial, and R. G. Parton.** 1996. Rab11 regulates recycling through the pericentriolar recycling endosome. J. Cell Biol. **135:**913–924.
57. **Ward, B. M., and B. Moss.** 2001. Vaccinia virus intracellular movement is associated with microtubules and independent of actin tails. J. Virol. **75:**11651–11663.
58. **Watanabe, R., and R. A. Lamb.** 2010. Influenza virus budding does not require a functional AAA+ ATPase, VPS4. Virus Res. **153:**58–63.
59. **Weisz, O. A., and E. Rodriguez-Boulan.** 2009. Apical trafficking in epithelial cells: signals, clusters and motors. J. Cell Sci. **122:**4253–4266.
60. **Wileman, T.** 2007. Aggresomes and pericentriolar sites of virus assembly: cellular defense or viral design? Annu. Rev. Microbiol. **61:**149–167.
61. **Wise, H. M., et al.** 2009. A complicated message: identification of a novel PB1-related protein translated from influenza A virus segment 2 mRNA. J. Virol. **83:**8021–8031.